Nuclear Materials and Energy 000 (2017) 1–7

Contents lists available at ScienceDirect

Nuclear Materials and Energy

journal homepage: www.elsevier.com/locate/nme

Mitigation of divertor heat flux by high-frequency ELM pacing with non-fuel pellet injection in DIII-D

A. Bortolon[a,*], R. Maingi[a], D.K. Mansfield[a], A. Nagy[a], A.L. Roquemore[a], L.R. Baylor[b], N. Commaux[b], G.L. Jackson[c], R. Lunsford[a], C.J. Lasnier[d], M.J. Makowski[d], R. Nazikian[a], T.H. Osborne[c], D. Shiraki[b], the DIII-D team

[a] Princeton Plasma Physics Laboratory, Receiving 3, Route 1 North, Princeton, NJ 08543 USA
[b] Oak Ridge National Laboratories, PO Box 2008, Oak Ridge TN 37831, USA
[c] General Atomics, 3550 General Atomics Ct., San Diego CA 92121, USA
[d] Lawrence Livermore National Laboratory, 7000 East Ave, P.O. Box 808, Livermore CA 94551, USA

ARTICLE INFO

Article history:
Received 22 July 2016
Revised 23 December 2016
Accepted 4 January 2017
Available online xxx

ABSTRACT

Experiments have been conducted on DIII-D investigating high repetition rate injection of non-fuel pellets as a tool for pacing Edge Localized Modes (ELMs) and mitigating their transient divertor heat loads. Effective ELM pacing was obtained with injection of Li granules in different H-mode scenarios, at frequencies 3–5 times larger than the natural ELM frequency, with subsequent reduction of strike-point heat flux (Bortolon et al., Nucl. Fus., 56, 056008, 2016). However, in scenarios with high pedestal density ($\sim 6 \times 10^{19}$ m^{-3}), the magnitude of granule triggered ELMs shows a broad distribution, in terms of stored energy loss and peak heat flux, challenging the effectiveness of ELM mitigation. Furthermore, transient heat-flux deposition correlated with granule injections was observed far from the strike-points. Field line tracing suggest this phenomenon to be consistent with particle loss into the mid-plane far scrape-off layer, at toroidal location of the granule injection.

1. Introduction

Unmitigated ELMs represent a potential threat for the divertor wall components of fusion devices like ITER, where, at full 15 MA operation, a projected 30–50x reduction may be required to avoid unacceptable damage [1]. Among the possible remedies, ELM pacing at frequencies much larger than the natural ELM frequency is of particular interest, as it also provides a direct tool to counteract the flux of high-Z impurities to the plasma core. Demonstration of ELM triggering by injection of frozen fuel (typically D_2) has been obtained in multiple devices [2,3], accompanied by reduction of ELM size proportional to the increase of ELM frequency. ELM 'acceleration' and mitigation has been also demonstrated with non-fuel pellets [4,5]. The use of non-fuel materials, in particular low Z, non-recycling materials, could contribute to reduce the gas load to the pumping and tritium processing systems for future devices. Here we report on experiments performed on DIII-D, where ELM mitigation by high-frequency pacing has been studied by injection of Li granules.

2. Apparatus and discharge scenario

Full-shot, high-frequency pacing of ELMs with non-fuel pellets was obtained in DIII-D using the lithium granule injector (LGI), a device capable of injecting solid granules of selectable size (0.3–1.0 mm diameter), with injection speed 50–120 m/s and average injection rates up to 100 Hz for 1.0 mm granules and up to 700 Hz for 0.3 mm granules. The LGI concept, implementation and diagnostic tools, are described in detail in [4,5]. For the experiments described here the LGI was located at toroidal angle 285°, injecting on a horizontal and approximately radial trajectory from the low field side mid-plane. The injection frequency was controlled by varying the potential applied to a piezoelectric disc, determining the approximate average rate at which granules are released from the selected reservoir, and fed to a rotating impeller. The injections were monitored by detecting the visible emission from the ablation cloud. The penetration depth of each granule is estimated from the duration of the ablation flash, during which strong magnetic

* Corresponding author.
E-mail address: abortolon@pppl.gov (A. Bortolon).

http://dx.doi.org/10.1016/j.nme.2017.01.003

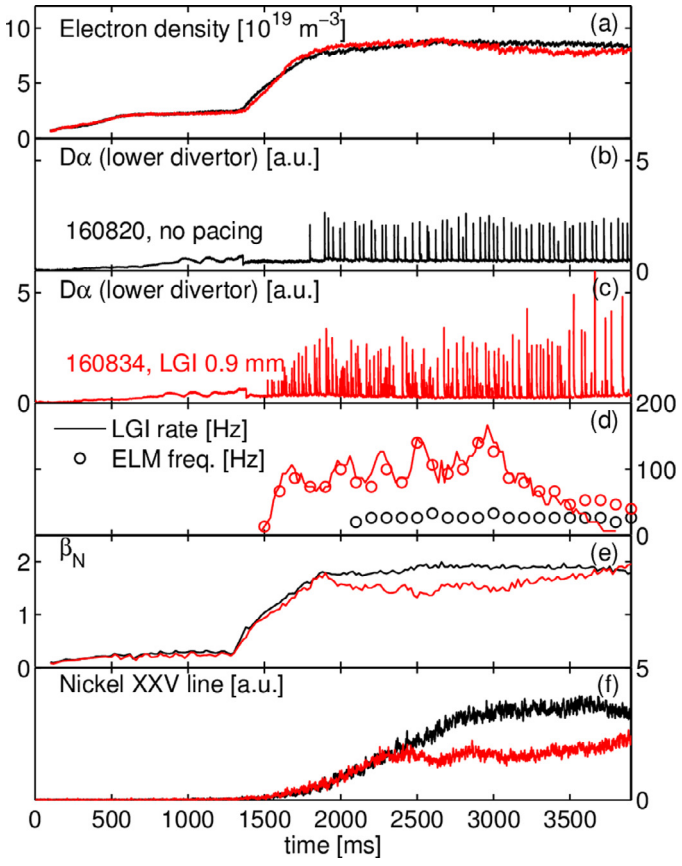

Fig. 1. Selected traces illustrating the discharge evolution for two discharges in ITER-baseline scenario, without (black) and with (red) Li granule injection. The evolution of Li granule injection rate and ELM frequency (d) are computed on a moving time interval of 150 ms. (For interpretation of the references to colour in this figure legend, the reader is referred to the web version of this article.)

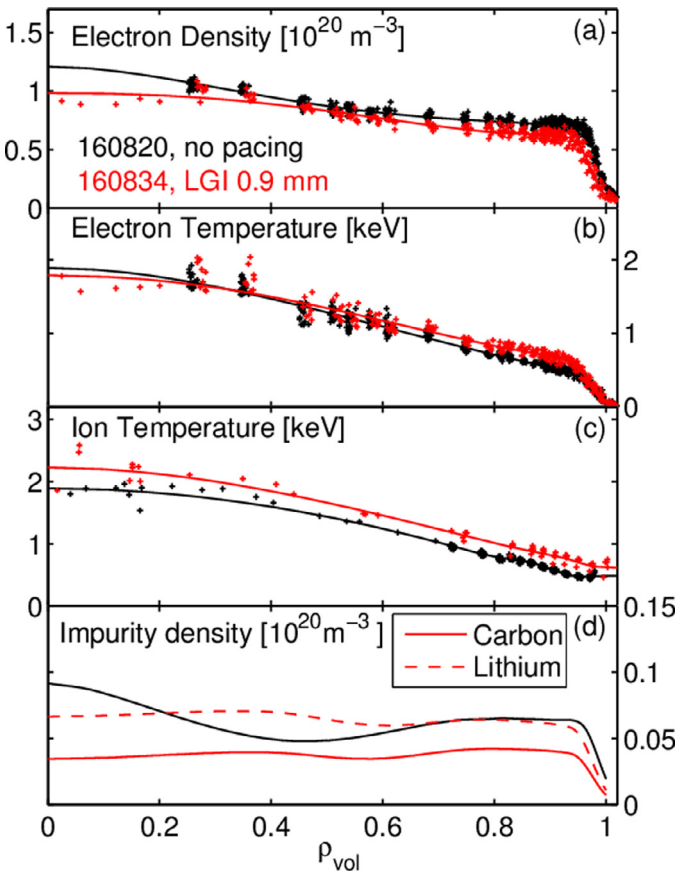

Fig. 2. Radial kinetic profiles, as a function of the normalized plasma volume, for a discharge with LGI pacing (160,834) and a reference discharge with uncontrolled ELMs (160,820). Experimental profiles are taken within 5 ms before ELM crashes.

fluctuations are also detected in the vicinity of the injection location. The granule penetration is inferred assuming constant velocity during the ablation: ablation times are measured in the range of 0.05–1.0 ms, corresponding to 0.5–10 cm penetration depth for granules of diameter 0.3–1 mm and injection velocity ~100 m/s [5,6]. Granule size and velocity can be selected to vary the amplitude and location of the applied perturbation, in order to maximize the ELM pacing effectiveness η_{trig}, defined as the number of ablation events divided by the number of triggered ELMs. An ELM is considered "triggered" when the beginning of the ELM spike in the divertor D_α emission occurs within 1 ms from the beginning of an ablation event.

The majority of the experiments discussed in this work were performed in deuterium plasmas, operated in the so called ITER-baseline scenario ($B_t = 1.6$ T, $I_p = 1.3$ MA, $\beta_N = 1.6$–1.9, $q_{95} = 3.1$, pedestal density $n_{e,ped} = 8.5 \times 10^{19}$ m^{-3}), with average ELM frequency $f_{ELM} = 28$ Hz in absence of pacing. The magnetic equilibrium is configured with the divertor inner strike point (ISP) on the central column, and the outer strike point (OSP) in the proximity of the cryo-pump baffle, to optimize active pumping and minimize density ramp up. At this relatively high plasma density, both strike points appear to be 'detached' between ELMs. A typical discharge evolution is represented in Fig. 1, for a reference discharge without pacing (160,820) and one with injection of 0.9 mm diameter Li granules, at 105 m/s (160,834). The injection begins at t = 1.5 s, and continues with variable rate between 80 and 150 Hz, up to 4 times larger than the natural ELM frequency (Fig. 1(d)). After t = 3 s, the injection frequency is gradually decreased to zero. The evolution of D_α emission from the lower divertor shows that the ELM activity begins earlier in the LGI discharge, as soon as the Li injection begins, and continues with frequency closely matching the Li granule injection rate (Fig. 1(d)). Indeed, by correlating ELM occurrence and ablation times, a triggering efficiency $\eta_{trig} \approx 100\%$ is found in these discharges. The D_α emission suggests a broader range of sizes for LGI paced ELMs, which, as discussed in the next section, is confirmed by measurements of drop of stored energy and divertor heat loads. Li injection appears contribute to the plasma electron inventory, as a reduced fueling rate is sufficient to match the requested target density. Li injection is found to reduce the accumulation of intrinsic metal impurities, as visible in Fig. 1(e), where Ni emission from the plasma core saturates at values 50% lower than the reference discharge. On the other hand, Li injection faster than 50 Hz, correlates with a moderate decrease in energy confinement. This is exemplified in Fig. 1(d), where, compared with $\beta_N = 1.8$ of the reference discharge, a reduced $\beta_N = 1.6$ is found at t = 2.0 s when $f_{LGI} \sim 150$ Hz, but increases to $\beta_N = 1.7$, at t = 3.5–3.8 s, when $f_{LGI} \sim 60$ Hz. Inspection of the kinetic profiles for the two discharges examined suggests that the decrease in energy confinement time τ_E is associated with changes in the pedestal, and not a change in core transport. Fig. 2 compares the radial profiles of electron density and temperature (n_e, T_e), ion temperature (T_i) and density of fully ionized carbon and lithium (n_C, n_{Li}). With Li pacing clear differences are observed at the pedestal top: a lower n_e corresponds to a 10% increase of T_e and T_i. On the other hand, the profiles propagate through the core with similar gradients, indicating similar magnitude of heat and particle transport. The higher temperatures measured at the pedestal top, might be a consequence of the 25% reduction in radiated power observed during LGI, from 2.4 to 1.8 MW.

Please cite this article as: A. Bortolon et al., Mitigation of divertor heat flux by high-frequency ELM pacing with non-fuel pellet injection in DIII-D, Nuclear Materials and Energy (2017), http://dx.doi.org/10.1016/j.nme.2017.01.003

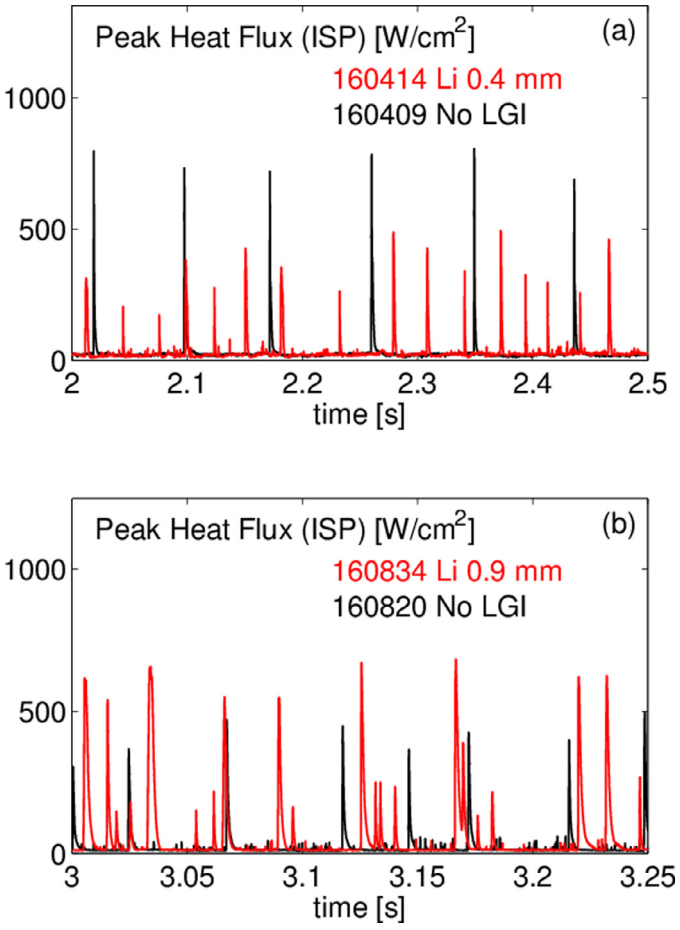

Fig. 3. Evolution of the peak heat flux measured at the inner strike point, for two plasma configurations: (a) β_N ~1.5, q_{95}~4.5 also discussed in Bortolon et al. [5] (b) β_N ~1.7, q_{95}~3.2, ITER-baseline scenario. Red traces correspond to discharges with Li injection and black traces show the corresponding reference discharges without ELM pacing. (For interpretation of the references to colour in this figure legend, the reader is referred to the web version of this article.)

3. Heat flux mitigation

In previous DIII-D experiments [5], ELM heat flux mitigation was obtained in discharges with Lower Single Null configuration, $B_t = 2.0$ T, $I_p = 1.2$ MA, $q_{95} = 4.6$, $\beta_N = 1.5$, $n_{e,ped} = 3.5$–4.5×10^{19} m^{-3}. Robust ELM pacing was documented for durations up to 3.5 s, with η_{trig}~100% obtained with granule diameter > 0.7 mm. η_{trig} dropped for smaller granule sizes, and was weakly dependent on granule velocity. Paced ELM frequencies up to 100 Hz were achieved (> 200 Hz transiently), with a 3–5 fold increase over the natural ELM frequency (12 Hz). Fig. 3(a), shows the evolution of the peak heat flux at ISP (denoted by q_{peak} in this work), for a discharge with LGI (0.4 mm diameter granules injection at ~100 m/s), and for a reference discharge with the same target parameters, without LGI. In the figure, all spikes correspond to ELMs; in the LGI discharge, all of these were triggered by a granule ablation event. In this case, LGI pacing increased f_{ELM} from 12 to 38 Hz, with a clear reduction of q_{peak} from 700 ± 50 W/cm^2 to 300 ± 100 W/cm^2, corresponding to 2–4X mitigation. Indeed, while $q_{peak} \sim 1/f_{ELM}$ was found at the OSP, the mitigation was weaker at the ISP, with q_{peak} often exceeding the $1/f_{ELM}$ relation.

Fig. 3(b) exemplifies the results obtained in subsequent experiments performed in the ITER-baseline scenario, described in Section 2, with lower q_{95}, torque and field, but higher pedestal density ($B_t = 1.6$ T, $n_{e,ped} = 8.5 \times 10^{19}$ m^{-3}). In this case also, all peaks in the LGI correspond to ELMs triggered by granule injections. However, although the LGI increased the ELM frequency from 20 to ~70 Hz, a much broader distribution of q_{peak} is found, characterized by a mix of small and large events. Notably, while q_{peak} was as low as 50 W/cm^2 for small events, the larger events had q_{peak}~600–800 W/cm^2, equal to or exceeding the values measured for natural ELMs. The data shown in Fig. 3 exemplifies the different response of the pedestal to ELM pacing obtained in the ITER-baseline scenario: while ELMs could be triggered at higher frequency, the mitigation of the ELM heat flux was not achieved.

The effectiveness of ELM mitigation can be studied by considering the distribution of size of ELM events in terms of drop in stored energy associated with each ELM crash, ΔW_{ELM}, and peak heat flux q_{peak}. Fig. 4 illustrates this for the ITER-baseline scenario ($\beta_N = 1.7$, $q_{95} = 3.1$) in two discharges with LGI, where ELM pacing at 100 Hz was obtained with 0.9 mm granule injected at 105 m/s and 60 m/s, and a reference discharge without LGI.

In the LGI discharges, both quantities are characterized by a much broader distribution extending from values close to zero to values 30% larger than in the reference discharge with natural unmitigated ELMs. For LGI-paced ELMs, the distribution of ΔW_{ELM} decreases monotonically, but a small fraction of events retains ΔW_{ELM} exceeding the average 25 kJ measured in the reference plasma. Interestingly, a substantially skewed q_{peak} distribution is found, that appears to combine two classes of events: 1) large ELMs, with $400 < q_{peak} < 600$ W/cm^2, and small ELMs with $10 < q_{peak} < 400$ W/cm^2.The distinction is more pronounced in the case of lower velocity injection, where a lower number of intermediate size ELMs is obtained and a larger fraction that shows $q_{peak} < 100$ W/cm^2. Notice that a number of events with $q_{peak} < 50$ W/cm^2, larger in the case of 60 m/s injections, occurs with the traits of a sub-threshold edge perturbation (STEP), i.e. energy and particle relaxation induced by granule ablations or other types of perturbations that did not trigger ELMs [5,7].

Fig. 5 shows the relation between ΔW_{ELM} and q_{peak}, for each ELM in the selected cases. For the class of larger LGI-paced ELMs ($q_{peak} > 300$ W/cm^2), the dependence of q_{peak} on ΔW_{ELM} is coarsely linear, with an off-set of ~300 W/cm^2. In particular, at the lower range $\Delta W_{ELM} < 10$ kJ, ELMs are observed with $300 < q_{peak} < 500$ W/cm^2. The figure includes data from the reference discharge, showing that LGI triggered ELMs have q_{peak} 30% larger than natural ELM of similar ΔW_{ELM}. The class of smaller amplitude events appears as a cluster of points with $\Delta W_{ELM} < 10$ kJ and $q_{peak} < 250$ W/cm^2. The separation between the two classes is clearer for the 60 m/s injection, suggesting that lower velocity is less effective for triggering intermediate amplitude events.

The reasons for this broad range of response to the granule injection are the object of present investigations. Differences in the applied perturbation, due e.g. to the intrinsic variability in granule mass, shape, velocity are thought to play a minor role, since similar indicators of granule ablation (e.g. ablation time, amplitude of magnetic perturbation or transient n_e increase) are found in conjunction with either large or small ELMs. In principle, non-periodic character of the LGI injection could result in a dynamic sequence of events of broadly varying amplitude. For instance, sporadic time histories as the one shown in Fig. 3(b), where large and infrequent ELMs are separated by frequent small events, might suggest a dynamic in which the small events delay the occurrence of large events, effectively decreasing the frequency of larger ELMs, and consequently increasing their size. However, the presence of large events after short wait-times (e.g. at t = 3.23 s) indicates that, in this scenario, the amplitude of the large triggered ELM weakly depends on the inter-ELM period. This is summarized in Fig. 6, where q_{peak} and ΔW_{ELM} are presented, for each ELM, as a function of the inverse of the wait time since the previous event. The graphs also include dashed lines to map the $1/f_{ELM}$ scaling of ELM

Please cite this article as: A. Bortolon et al., Mitigation of divertor heat flux by high-frequency ELM pacing with non-fuel pellet injection in DIII-D, Nuclear Materials and Energy (2017), http://dx.doi.org/10.1016/j.nme.2017.01.003

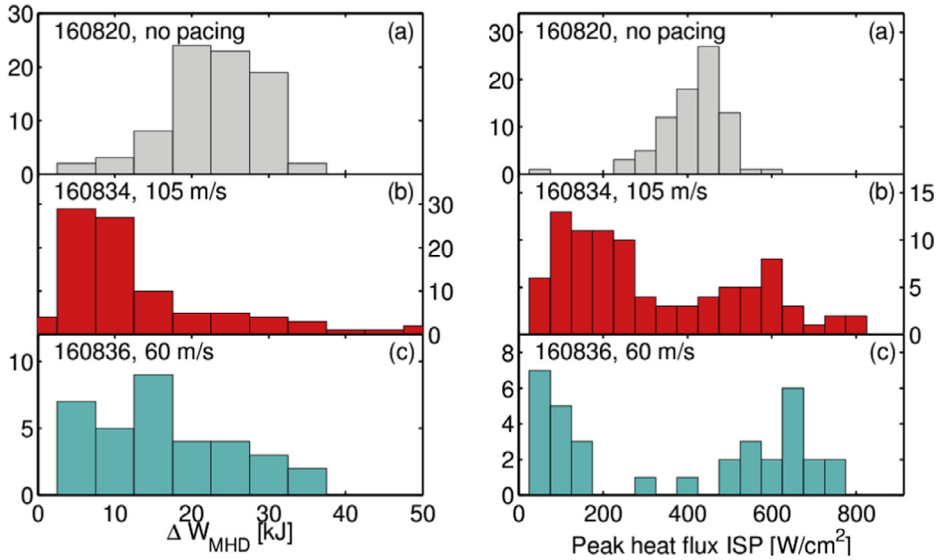

Fig. 4. Distribution of ELM stored energy loss ΔW_{ELM} (left) and ISP peak heat flux (right) measured in ITER-baseline plasmas without pacing (a), with injection of 0.9 mm Li granules at 105 m/s (b) and 60 m/s (c).

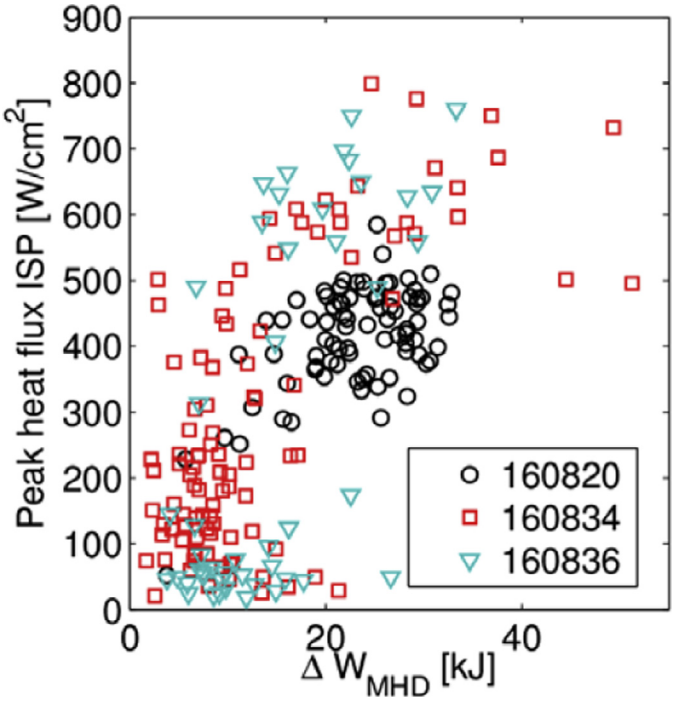

Fig. 5. ELM peak heat flux at the inner strike point as a function of drop in stored energy for the discharges showed in Fig. 4 (160,834, 105 m/s; 160,836, 60 m/s; 160,820 reference without pacing).

amplitude, normalized to the reference discharge data [8]. A tendency emerges in the dataset of smaller ELM size at shorter ELM wait time, coarsely aligned with the $1/f_{ELM}$ relation. However, a substantial spread exists at any value of $1/\Delta t_{ELM}$, indicating that the dependence of ELM amplitude or q_{peak} on Δt_{ELM} (or f_{ELM}) is weak. As a result, the $1/f_{ELM}$ expectation appears violated, even at values of ELM frequency 5× larger that the natural ELM frequency. Notice that these results, obtained in the ITER-baseline scenario, are in contrast with the observations reported in Bortolon et al. [5] for Li pellet injection and summarized at the beginning of this section. The causes of the different behavior are subject of active investigation, and are likely associated with the different pedestal characteristics (e.g. n_e, T_e, q_{95}), influencing both ELM stability and granule penetration.

4. Heat flux footprint

To investigate the difference of distribution of ELM energy loss and heat loads, the spatial structure of the divertor ELM heat flux was measured. The radial profile of q_{div} in vicinity of the ISP is determined by applying heat conduction modeling to high-speed infra-red thermography measurements from a vertical view of the divertor, at toroidal angle 60° [9]. Fig. 7(a) shows the maximum q_{div} achieved at each radial location during three selected ELMs. The figure compares a natural ELM from discharge 160,820 (reference) with a large and a small Li-triggered ELM from discharge 160,834 (0.9 mm, 105 m/s). The figure includes also the inter-ELM profile, characterized by the absence of localized heat-flux features, indicative of divertor detachment at the inner leg. Both natural and LGI triggered ELMs are characterized by a single peak at the ISP. (At the OSP, due to the geometrical limitation of the IR camera coverage, the presence of a secondary peak cannot be excluded but is considered unlikely.) The two Li-triggered ELMs, although separated by a factor of ~5 in q_{peak}, do not show significantly different profile features. The comparison between the natural ELM and the Li-triggered ELM with similar q_{peak}~400 W/cm^2 (red) exemplifies the narrower deposition observed for LGI events (full-width half-maximum FWHM~14 cm) compared to natural ELMs (FWHM~21 cm). This difference can be evaluated in terms of ELM wetted area, defined as $A_w = P_{div}/q_{peak}$, where P_{div} is the power deposited in the vicinity of the strike point [10], determined by integrating q_{div} radially and toroidally, assuming axisymmetry. Indeed, Fig. 7(b) shows that, in the range of q_{peak}~350–500 W/cm^2, A_w is systematically smaller by ~20–30% in LGI discharge (A_w~1.4 m^2) compared to the reference discharge (A_w~1.8 m^2). Such a reduction might contribute to the higher q_{peak} found for LGI ELMs compared to natural ELMs, for similar ELM energy loss (Fig. 5). The origin of this different behavior is under study, and might result, for instance, from the spatial structure of the magnetic instabilities leading to natural or paced ELMs [10,11], or from changes in divertor conditions, typically characterized by lower neutral density and radiation losses in LGI discharges.

Information on the heat load structure on a larger spatial domain was available from a tangential wide angle IR imaging, of-

Please cite this article as: A. Bortolon et al., Mitigation of divertor heat flux by high-frequency ELM pacing with non-fuel pellet injection in DIII-D, Nuclear Materials and Energy (2017), http://dx.doi.org/10.1016/j.nme.2017.01.003

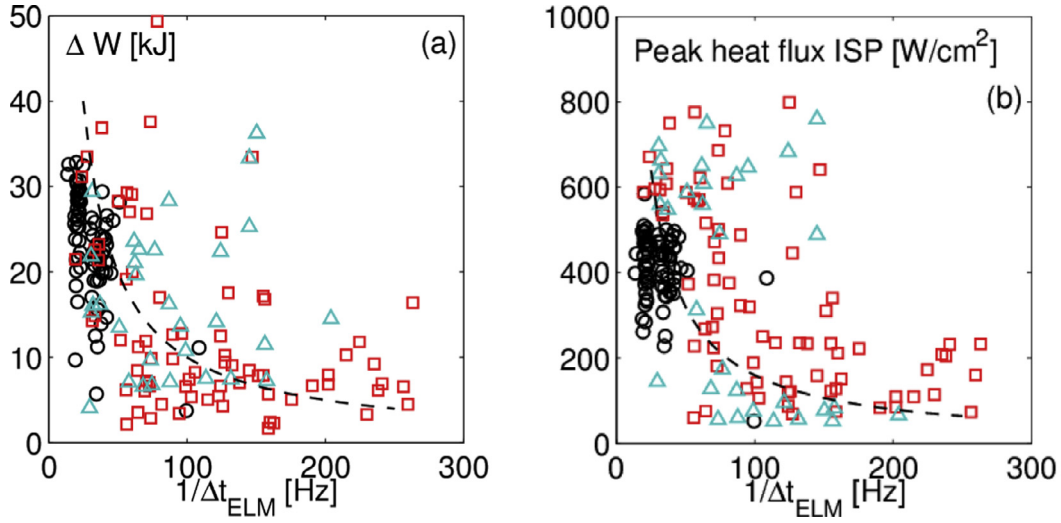

Fig. 6. Statistical representation of plasma stored energy drop (a) and peak heat flux at the inner strike point (b), for the discharges in Fig. 5. Data are shown for each ELM event as a function of the inverse of the pre-ELM period. Dashed lines show a constant/f_{ELM} curve, normalized to the reference discharge data.

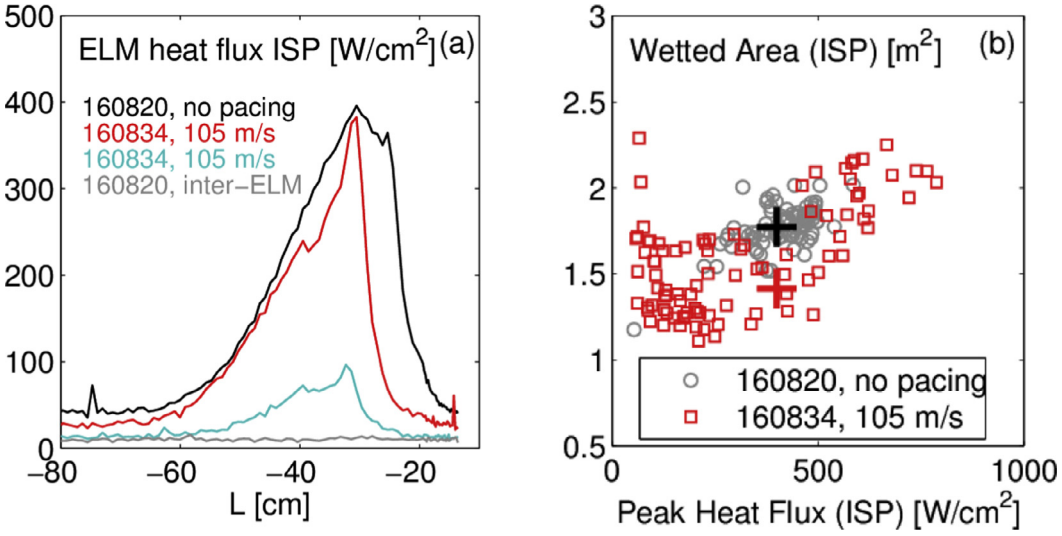

Fig. 7. (a) Profile of the maximum heat flux measured in the proximity of the ISP, during a selection of ELM events, as a function of the linear spatial coordinate L, which measures distances along the wall poloidal cross-sections, including a natural ELM (black) and two Li-triggered ELMs (red, cyan) of different magnitude. (b) Wetted area measured at the ISP for ELMs in two discharges with and without LGI pacing. Crosses indicate average values for $350 < q_{peak} < 450$ W/cm^2; for ELM of similar amplitude the wetted area is 20% smaller for LGI paced ELMs. (For interpretation of the references to colour in this figure legend, the reader is referred to the web version of this article.)

fering a toroidal coverage of the lower divertor of ~90° (toroidal machine angle 115–195°) [12]. The wide angle IR camera data documented robustly transient striations as far as 20 cm away from the outer strike-point (Fig. 8(a)). These striations are clearly visible for LGI triggered events in frames taken within 0.2 ms from the beginning of the granule ablation, unrelated to the size of the triggered ELM. In the lower divertor they appear at R = 1.55–1.60 m, on the so called 'lower divertor shelf'. The absence of heat flux deposition at this radial location in the measurements from the vertical fast IR camera, located at 60°, suggests that this striation is toroidally asymmetric. Notably, similar observations have been reported from JET during experiments of D_2 pellet injections, where field line tracing from the injection location to the divertor plates suggested a possible dominant transport component into the SOL crossing separatrix at the injection location [13]. For the cases presented in this work, field line tracing calculations show that field lines originating at the LGI toroidal location between the plasma boundary and the outer wall tiles connect to the lower divertor on the shelf, in an arc of spiral depicted by the red line in Fig. 8(b). The toroidal extension of the arc is associated with the radial location of the field line origins on the equatorial plane: field lines originating close to wall tiles hit the shelf at ~230°, and the hit location shifts counter-clockwise for field lines closer to the plasma boundary. Field aligned transport of plasma expelled into the far scrape-off layer (SOL) at the granule injection location, possibly in form of filaments, would deposit heat and particles along the red line. While thermography analysis estimates a typical surface temperature increase of 50–100 °C at the tile surface, the low framing rate (~15 Hz) does not allow the reconstruction of the ELM-resolved heat load associated with these features.

5. Discussion

The use of non-fuel, non-recycling materials as pellets represent a new tool in ELM control research, providing a high degree of flexibility to achieve high injection frequencies. In the case of Li, main chamber recycling is unaffected and electron density and collisionality are maintained. While the relative densities of the injected

Please cite this article as: A. Bortolon et al., Mitigation of divertor heat flux by high-frequency ELM pacing with non-fuel pellet injection in DIII-D, Nuclear Materials and Energy (2017), http://dx.doi.org/10.1016/j.nme.2017.01.003

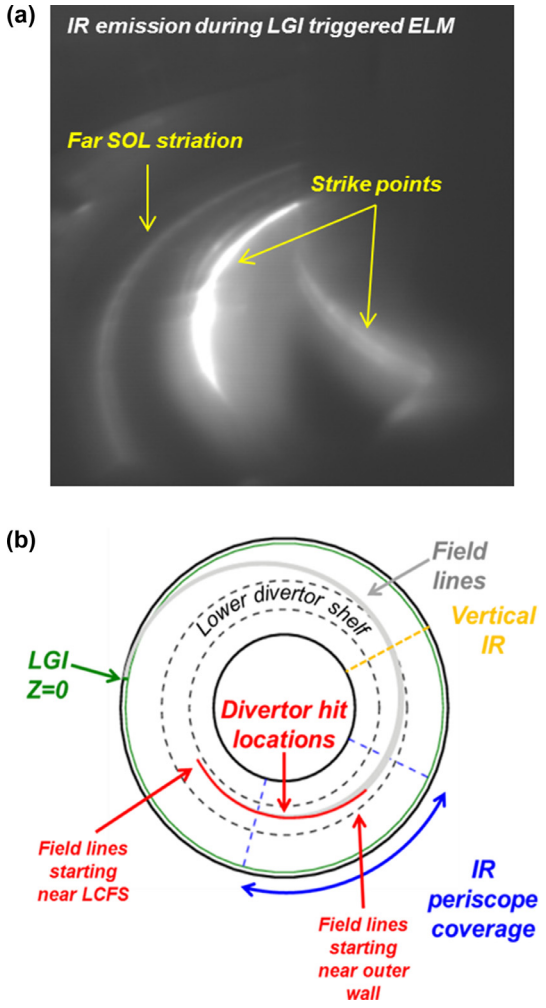

Fig. 8. (a) IR emission from the lower divertor during an ELM generated by a Li granule injection; striations are observed on the divertor shelf, 15–25 cm outside the outer strike point. (b) Top view of the lower divertor, including field lines traced from the far SOL at the location of granule injection, down to the lower divertor. The dashed lines indicate the inner and outer edges of the divertor shelf. Field-line hit locations map into a spiral consistent with the structure observed in the IR images.

impurity can grow relatively high, the reduction of higher Z contaminants (e.g. C) results in a modest increase (<10%) of even decrease of Z_{eff}. [5]. The recent dataset, acquired in the ITER-baseline scenario plasmas with Li granule injection, provides new insights on the field of ELM pacing and mitigation. The scenario incorporates several similarity aspects with the ITER case, in particular in terms of shape, pedestal density and applied torque. With LGI injection in this scenario, high pacing efficiency has been achieved, close to 100%, when including all pedestal relaxations induced by granule ablation events. However, a small fraction of the ELMs, retain a q_{peak} that is similar to or larger than the natural, uncontrolled ELMs. This finding holds true even when the ELM frequency is increased by a factor of 3-5 compared to the natural ELM frequency. This phenomenon poses a real challenge for the prospect of heat load mitigation by high frequency ELM pacing. It must be noted that this type of evidence has not been observed in DIII-D, applying D_2 and Li pellets to different scenarios [3,5], indicating that this phenomenology might be specific to the experimental conditions. In particular the use of deeply penetrating Li pellets, needed to achieve high pacing frequencies in these high pedestal density plasmas, together with the non-periodical injection sequences could possibly result in a more spatially extended, and less repeatable MHD events. Interestingly observations of weak dependence of ELM amplitude on inter-ELM period in ITER-baseline scenario have been recently reported in JET ELM pacing with relatively large D_2 pellets [14]. Also, a similar phenomenology was documented in DIII-D discharges at high collisionality, where ELM frequency was increased by means of modulated 3D fields [15]. These observations call for clear resolution, since it is legitimate to expect that larger pellet induced perturbations would be required to achieve the highest 30–50X f_{ELM} multiplication, especially in scenarios prone to "lag times" issues [16]. In this respect, advanced modeling is needed to determine the non-linear dynamic evolution of the triggered ELM, to understand 1) the characteristics of ELM crash under the pedestal properties typical of LGI plasma, e.g. collisionality; 2) the non-linear dynamic evolution of the triggered ELM. Such modeling has recently been initiated using the M3D-C[1] code [17], recently extended to include localized particle sources from ablating Li granules [18].

Acknowledgment

Supported in part by U.S. Dept. of Energy under contracts DE-AC02-09CH114661, DE-AC05-00OR227252, DE-FC02-04ER546983, DE-FG02-06ER54867 and DE-AC52-07NA273444. DIII-D data shown in this paper can be obtained in digital format by following the links at https://fusion.gat.com/global/D3D_DMP.

References

[1] A. Loarte, G. Huijsmans, S. Futatani, L.R. Baylor, T.E. Evans, D.M. Orlov, O. Schmitz, M. Becoulet, P. Cahyna, Y. Gribov, A. Kavin, A. Sashala Naik, D.J. Campbell, T. Casper, E. Daly, H. Frerichs, A. Kischner, R. Laengner, S. Lisgo, R.A. Pitts, G. Saibene, A. Wingen, Progress on the application of ELM control schemes to ITER scenarios from the non-active phase to DT operation, Nucl. Fusion 54 (3) (2014) 033007.
[2] P.T. Lang, G.D. Conway, T. Eich, L. Fattorini, O. Gruber, S. Gunter, L.D. Horton, S. Kalvin, A. Kallenbach, M. Kaufmann, G. Kocsis, A. Lorenz, M.E. Manso, M. Maraschek, V. Mertens, J. Neuhauser, I. Nunes, W. Schneider, W. Suttrop, H. Urano, the ASDEX Upgrade Team, ELM pace making and mitigation by pellet injection in ASDEX upgrade, Nucl. Fusion 44 (5) (2004) 665.
[3] L.R. Baylor, N. Commaux, T.C. Jernigan, N.H. Brooks, S.K. Combs, T.E. Evans, M.E. Fenstermacher, R.C. Isler, C.J. Lasnier, S.J. Meitner, R.A. Moyer, T.H. Osborne, P.B. Parks, P.B. Snyder, E.J. Strait, E.A. Unterberg, A. Loarte, Reduction of edge-localized mode intensity using high-repetition-rate pellet injection in tokamak H-mode plasmas, Phys. Rev. Lett. 110 (Jun) (2013) 245001.
[4] D.K. Mansfield, A.L. Roquemore, T. Carroll, Z. Sun, J.S. Hu, L. Zhang, Y.F. Liang, X.Z. Gong, J.G. Li, H.Y. Guo, G.Z. Zuo, P. Parks, W. Wu, R. Maingi, First observations of ELM triggering by injected lithium granules in EAST, Nucl. Fusion 53 (11) (2013) 113023.
[5] A. Bortolon, R. Maingi, D.K. Mansfield, A. Nagy, A.L. Roquemore, L.R. Baylor, N. Commaux, G.L. Jackson, E.P. Gilson, R. Lunsford, P.B. Parks, C. Chrystal, B.A. Grierson, R. Groebner, S.R. Haskey, M.J. Makowski, C.J. Lasnier, R. Nazikian, T. Osborne, D. Shiraki, M.A. Van Zeeland, High frequency pacing of edge localized modes by injection of lithium granules in DIII-D H-mode discharges, Nucl. Fusion 56 (5) (2016) 056008.
[6] R. Lunsford, A. Bortolon, A.L. Roquemore, D.K. Mansfield, A. Nagy, R. Maingi, P.B. Parks, G. Jackson, E. Gilson, C.P. Chrobak, Lithium granule ablation and penetration during ELM pacing experiments at DIII-D, J. Fusion Eng. Design 12 (2016) 621–627.
[7] J.D. Lore, J.M. Canik, J.-W. Ahn, A. Bortolon, E.D. Fredrickson, M.A. Jaworski, G.J. Kramer, R. Maingi, A.G. McLean, F. Scotti, V.A. Soukhanovskii, K. Tritz, Effect of n = 3 perturbation field amplitudes below the ELM triggering threshold on edge and SOL transport in NSTX, in: Proceedings of the 20th International Conference on Plasma-Surface Interactions in Controlled Fusion Devices, J. Nucl. Mater. 438 (Supplement(0)) (2013) S388–S392.
[8] L.R. Baylor, N. Commaux, T.C. Jernigan, S.J. Meitner, S.K. Combs, R.C. Isler, E.A. Unterberg, N.H. Brooks, T.E. Evans, A.W. Leonard, T.H. Osborne, P.B. Parks, P.B. Snyder, E.J. Strait, M.E. Fenstermacher, C.J. Lasnier, R.A. Moyer, A. Loarte, G.T.A. Huijsmans, S. Futatani, Reduction of edge localized mode intensity on DIII-D by on-demand triggering with high frequency pellet injection and implications for ITER, Phys. Plasmas 20 (8) (2013) 082513.
[9] D.N. Hill, R. Ellis, W. Ferguson, D.E. Perkins, T. Petrie, C. Baxi, Infrared thermography of the DIII-D divertor targets, Rev. Sci. Instrum. 59 (8) (1988) 1878–1880.
[10] J.-W. Ahn, R. Maingi, J.M. Canik, K.F. Gan, T.K. Gray, A.G. McLean, Broadening of divertor heat flux profile with increasing number of ELM filaments in NSTX, Nucl. Fusion 54 (12) (2014) 122004.
[11] J.-W. Ahn, G.P. Canal, S.K. Kim, J.M. Canik, Effect of pedestal stability regime on the behavior of ELM heat flux footprints in NSTX and DIII-D, in: PSI Conference, 2016.

Please cite this article as: A. Bortolon et al., Mitigation of divertor heat flux by high-frequency ELM pacing with non-fuel pellet injection in DIII-D, Nuclear Materials and Energy (2017), http://dx.doi.org/10.1016/j.nme.2017.01.003

[12] C.J. Lasnier, S.L. Allen, R.E. Ellis, M.E. Fenstermacher, A.G. McLean, W.H. Meyer, K. Morris, L.G. Seppala, K. Crabtree, M.A. Van Zeeland, Wide-angle ITER-prototype tangential infrared and visible viewing system for DIII-D, Rev. Sci. Instrum. 85 (11) (2014).
[13] RP Wenninger, TH Eich, GTA Huysmans, PT Lang, S Devaux, S Jachmich, F Kochl, JET EFDA Contributors, Scrape-off layer heat transport and divertor power deposition of pellet-induced edge localized modes, Plasma Phys. Control. Fusion 53 (10) (2011) 105002.
[14] IT Chapman, E de la Luna, PT Lang, Y Liang, B Alper, P Denner, D Frigione, L Garzotti, CJ Ham, GTA Huijsmans, S Jachmich, G Kocsis, M Lennholm, I Lupelli, FG Rimini, ACC Sips, JET Contributors, Advances in understanding and utilising ELM control in JET, Plasma Phys. Control. Fusion 58 (1) (2016) 014017.
[15] W.M. Solomon, K.H. Burrell, A.M. Garofalo, R.J. Groebner, C.J. Lasnier, M.A. Makowski, T.H. Osborne, H. Reimerdes, J.S. deGrassie, E.J. Doyle, T.E. Evans, M.E. Fenstermacher, G.L. Jackson, M.J. Schaffer, ELM pacing using modulated non-axisymmetric magnetic fields on DIII-D, Nucl. Fusion 52 (3) (2012) 033007.
[16] P.T. Lang, D. Frigione, A. Geraudraudraud, T. Alarcon, P. Bennett, G. Cseh, D. Garnier, L. Garzotti, F. Kochl, G. Kocsis, M. Lennholm, R. Neu, R. Mooney, S. Saarelma, B. Sieglin, JET-EFDA Contributors, ELM pacing and trigger investigations at JET with the new ITER-like wall, Nucl. Fusion 53 (7) (2013) 073010.
[17] N.M. Ferraro, S.C. Jardin, Calculations of two-fluid magnetohydrodynamic axisymmetric steady-states, J. Comput. Phys. 228 (20) (2009) 7742–7770.
[18] A. Fil, E. Kolemen, N. Ferraro, A. Bortolon, D. Eldon, P.B. Parks, S. Jardin, R. Lunsford, R. Maingi, Modeling of ELM-pacing by lithium granule injection with M3D-C^1, in: PSI Conference, 2016.

Please cite this article as: A. Bortolon et al., Mitigation of divertor heat flux by high-frequency ELM pacing with non-fuel pellet injection in DIII-D, Nuclear Materials and Energy (2017), http://dx.doi.org/10.1016/j.nme.2017.01.003